

Effect of Sn doping concentration on structural, optical and electrical properties of ZnS/p-Si (111) diodes fabricated by sol-gel dip-coating method

Şirin Uzun Çam ^{a,*}, Tülay Serin ^b, A. Necmeddin Yazıcı ^a

^a Department of Engineering Physics, Faculty of Engineering, Gaziantep University, 27310, Gaziantep, Turkey

^b Department of Engineering Physics, Faculty of Engineering, Ankara University, 06100, Ankara, Turkey



ARTICLE INFO

Keywords:

ZnS
Diode
Sol-gel
p-Si
Sn doped
Photosensitivity

ABSTRACT

Tin doped zinc sulfide (ZnS:Sn) thin films have been fabricated by sol-gel dip-coating method on glass and p-Si substrates by varying Sn concentration between 0 wt % and 10 wt %. The structural and optical properties of ZnS:Sn thin films have been studied by X-ray diffraction and spectrophotometer measurements. X-ray results show the films grown on glass and p-Si substrate are cubic structure. Optical band gap values found from the transmittance spectra have decreased from 3.58 eV to 3.42 eV with the addition of Sn. The effect of tin concentration on the device performance of ZnS:Sn/p-Si has been investigated through the analysis of the I-V characteristics under dark and illuminated conditions. Diode parameters such as ideality factor n , barrier height ϕ_b , saturation current I_0 , series resistance value R_s have been calculated by means of thermionic emission theory, and Norde method. Photosensitivity PS , photoresponsivity R , and detectivity D values of the diodes have been determined from I-V measurements under 100 mW/cm² illumination intensity. It has been determined that 3% Sn doped ZnS/p-Si diode showed the best diode and photodiode properties among Sn doped ZnS/p-Si diodes.

1. Introduction

ZnS is a promising semiconductor material for optoelectronic applications, particularly for photovoltaics due to its large absorption coefficient ($\alpha > 10^4 \text{ cm}^{-1}$) [1,2]. ZnS, the compound II-VI, exhibits n-type semiconductor properties with a wide and direct band gap in the 3.5–3.9 eV range [3,4]. ZnS can crystallize such as cubic phase or hexagonal wurtzite form [5]. In addition, low-cost, nontoxicity, stability, and environmentally friendly are other important features of ZnS [6]. In order to modify the electrical and optical properties of a pure semiconductor that affect device performance, doping is an efficient method. Many researchers have tried to enhance the physical performance of ZnS film by adding different dopant atoms for instance Al, Sn, Mn, Cu [7–10].

ZnS thin films can be manufactured by many deposition techniques such as; sol-gel spin coating [11], chemical bath deposition (CBD) [12], spray pyrolysis [13], RF sputtering [14], pulsed laser deposition [15], chemical vapor [16], molecular beam epitaxy [17] etc.

The few studies in the literature on ZnS/Si are as follows. Al-doped ZnS/p-Si (100) prepared CBD was studied and photoluminescence

properties of structures were reported in Ref. [18]. Similarly, Al-doped ZnS/p-Si was reported and using C-V measurement built-in potential and ideality factor were calculated [19]. ZnS/Si isotype heterojunction was prepared and photodiode characteristics were investigated [20]. Using CBD technique ZnS/p-Si heterojunction was obtained and photovoltaic characteristic was studied [21–23]. ZnS grown on p-Si (100) was annealed 500 °C at 2 h and it was reported that good rectifying behaviour was observed [24].

In this study, the effect of tin concentration, which is rarely encountered in the literature, on ZnS:Sn/p-Si device performance was investigated by the analysis of I-V properties. Undoped and Sn doped ZnS films were coated on glass and Si substrates using the sol-gel method because the added atoms distribute in the coating solution as homogeneously. The reason why tin was chosen as the dopant is ionic radii value. Ionic radii of the Sn⁴⁺ is 0.071 nm and ionic radii of the Zn²⁺ is 0.074 nm [25,26]. On the other hand, ionic radii values of some dopants such as Al³⁺, In³⁺, Mn²⁺, and Cu²⁺ are 0.051 nm, 0.080 nm, 0.083 nm, and 0.073 nm, respectively [27–29]. If we compare ionic radii values with each other we will see that ionic radii values of Sn⁴⁺ and Cu²⁺ are very close to that of Zn²⁺. Thus, we can say using Sn and Cu as dopants

* Corresponding author.

E-mail addresses: sirinuzun@gantep.edu.tr (Ş. Uzun Çam), serin@eng.ankara.edu.tr (T. Serin), yazici@gantep.edu.tr (A.N. Yazıcı).

may cause less lattice defect than the others. In addition, Sn has four valence electrons and this provides extra electrons for the electrical conduction. Thus, Sn can be an effective dopant for ZnS structure.

2. Experimental details

In this study, the films were prepared using the sol-gel dip-coating method. For undoped ZnS films, we prepared two solutions as the main solution. Zinc acetate dihydrate ($\text{Zn}(\text{CH}_3\text{COO})_2 \cdot 2\text{H}_2\text{O}$) and thiourea ($\text{CH}_4\text{N}_2\text{S}$) were dissolved in methanol (CH_4O) molar ratio 1:3, separately. Zinc acetate solution was started to stir on a magnetic stirrer. Thiourea solution was added into the solution afterwards and it was blurred. We obtained a clear solution by adding ethanolamine ($\text{C}_2\text{H}_7\text{NO}$). For Sn doped films, tin chloride ($\text{SnCl}_2 \cdot 2\text{H}_2\text{O}$) was added. Sn/Zn ratio was varied from 0 to 10 wt%. The mixed solution was stirred totally 2 h on a magnetic stirrer and was aged 24 h before the coating process. The solution preparing process was carried out at room temperature. Glass and p-type Si (111) wafer were used as substrate.

Before coating, glass substrates were cleaned in ethanol and de-ionized water in an ultrasonic cleaner. Si substrates were cleaned by RCA cleaning technique. Firstly, the substrates were dipped in a 65 °C solution of $\text{NH}_4\text{OH}:\text{H}_2\text{O}_2:\text{H}_2\text{O}$ (1:1:5) for 10 min. Secondly, they were cleaned in $\text{HF}:\text{H}_2\text{O}$ (1:10) solution for 30 s to remove the oxide layer on the wafer. Finally, they were dipped in a 65 °C solution of $\text{HCl}:\text{H}_2\text{O}_2:\text{H}_2\text{O}$ (1:1:6) for 10 min. After all cleaning steps, p-Si substrates were rinsed in de-ionized water for 30 s. Then, high-purity Al (99.999%) was evaporated from the tungsten filament onto the whole back surface of the p-Si substrates under the pressure 10^{-6} Torr as thermally. p-Si substrates were annealed at 580 °C for 10 min to get a low-resistivity ohmic back contact.

Both p-Si and glass substrates were dipped vertically in the solution with a velocity of 3 mm/s and were removed from the solution with the same velocity immediately after. After the coating process, the films were dried at 300 °C for 5 min in the air. The coating process was repeated 15 times for glass and 6 times for p-Si substrates to increase film thickness. Then, the films were annealed at 500 °C in a vacuum for 1 h. It is well-known that in the case of $\Phi_M < \Phi_S$, the metal-semiconductor contact is ohmic if the semiconductor is n-type. Therefore, since ZnS is an n-type semiconductor material with the electron affinity and work function are 3.90 eV [30] and 5.1 eV [31] it forms an ohmic contact with Al ($\Phi_M = 4.28\text{eV}$ [32]). Finally, the high-purity Al-ohmic contacts were coated on ZnS films coated on p-type silicon by thermal evaporation method and using a circular-shaped mask with the area of 0.025 cm^2 . This coating was carried out in high vacuum evaporation system under the pressure of 10^{-6} Torr.

The structural analysis of Sn doped ZnS was investigated with X-ray diffraction (XRD). XRD measurements were performed by Rikagu Miniflex 600 Table Top Powder X-Ray diffractometer using $\text{CuK}\alpha$ radiation source ($\lambda = 0.15406\text{ nm}$) in the 2θ scanning range of 20° – 60° . The optical transmission (T%) and reflection (R%) measurements of the material were obtained in the UV–Vis–NIR range by Shimadzu 3600 spectrophotometer in the wavelength range of 300–1800 nm. In order to detect elemental ratios in the composition, EDX analysis was carried using Hitachi SU5000 Schottky FE-SEM instrument. Film thicknesses were also found from SEM images taken using the same device. Current-voltage (I–V) measurement of Sn doped ZnS/p-Si structure was performed in the dark and under illumination using Keithley 2420 programmable constant current source at room temperature. Illuminated current-voltage (I–V) measurement was done under 100 mW/cm^2 illumination intensity using AM 1.5 filter.

3. Results and discussions

3.1. Structural properties

XRD spectra of the Sn doped ZnS films on silicon and glass substrates

are given in Fig. 1 and Fig. 2, respectively. According to Fig. 1, the strongest diffraction peak was observed at $2\theta = \sim 28^\circ$, corresponding both (111) cubic structure of ZnS and (111) Si crystal [33,34]. The intensity of the cubic ZnS is much smaller than that of the Si crystal reflection. Thus, the reflection of the cubic ZnS is shown in the figure as the inset graph in Fig. 1.

It can be seen from Fig. 2 that ZnS films on glass crystallized in the cubic structure. Increasing dopant concentration caused one more diffraction peak from (220) of the cubic structure of ZnS. However, the intensity of the main diffraction peak reduced with increased dopant concentration. It can be said that 10% Sn doped ZnS thin film has an amorphous structure. Increased dopant concentration has changed the structural features of the films. Similar result was reported in Ref. [35]. They studied the doping effect of Sn doped ZnO thin films. They said that the main diffraction peak increased with increasing dopant concentration until 0.6% but it decreased the dopant concentration by 1%. The other study reported that 10% and 15% Sn doping concentration decreased the intensity of the peaks (100) and (002) for the hexagonal reflections [36]. In another study about the Cu doped ZnS thin films, while pure ZnS thin film has a cubic structure with (111) reflection, adding Cu dopant (0.05%) caused amorphization of the films [37]. As a result, we can say that the films grown on glass and p-Si substrate have a cubic structure. Deposition conditions affect the structural properties of the ZnS thin films. While the ZnS films are grown under vacuum they crystallize as the cubic form, the films are grown under N_2 gas they form hexagonal wurtzite [38]. Thus, our result is in agreement with this report.

Using Debye-Scherrer's Formula the mean crystallite size of structures was calculated for the strongest peak corresponding to (111) orientation.

$$D = \frac{0.94\lambda}{\beta \cos \theta} \quad (1)$$

Where D is the mean crystallite size, λ is the wavelength of $\text{CuK}\alpha$ radiation (0.15406 nm), β is the full width at half maximum (FWHM) of the strongest diffraction peak and θ is the Bragg's angle. In addition, the inter-planar spacing d_{hkl} values were calculated using Bragg's Law and lattice constant was calculated for the cubic phase using equation (3).

$$\lambda = 2d_{hkl} \sin \theta_{hkl} \quad (2)$$

$$d_{hkl} = \frac{a}{\sqrt{h^2 + k^2 + l^2}} \quad (3)$$

Lattice mismatch values are obtained equation (4) [39].

$$\frac{\Delta a}{a} = \frac{2(a_2 - a_1)}{(a_2 + a_1)} \quad (4)$$

Where a_1 and $a_2 = 0.54309\text{ nm}$ are the lattice constants of the Sn doped ZnS films and p-Si crystal, respectively. The obtained 2θ , the mean crystallite size D , the inter-planar spacing value d_{hkl} , lattice constant a , and lattice mismatch values of Sn doped ZnS structures are given in Table 1. Lattice mismatch values are under 1% and we can say the interface defects are decidedly minimal. Our results are in good agreement with reported results [40].

Fig. 3 shows EDX spectra of undoped and Sn doped ZnS thin films. The spectrum reveals the presence of Zn, S and Sn elements in the deposited film. At the same time, it is seen from Fig. 3 that while Sn concentration increases, Zn decreases.

The thicknesses of undoped and Sn doped ZnS thin films were found from cross-sectional SEM images as shown Fig. 4. These values are given in Table 2.

3.2. Optical properties

The optical transmittance and reflectance spectra of the films are

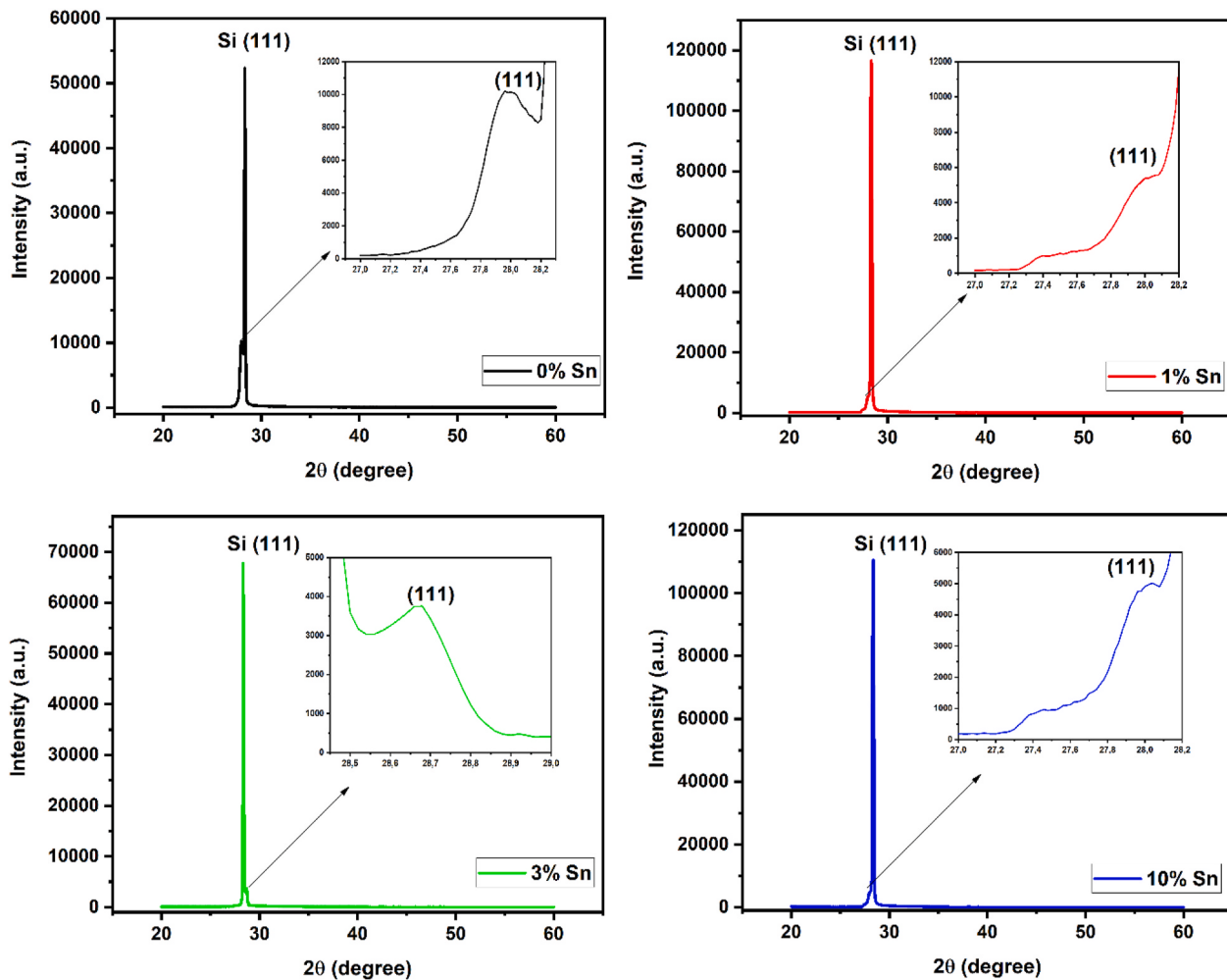


Fig. 1. XRD pattern of Sn doped ZnS/p-Si structures. Inset graphs give the peak of cubic ZnS.

given in Fig. 5. The films have very high transparency and it decreases with increased dopant concentration. For instance, the optical transmittance value decreased from 85% to 65% in the visible range. Since even 65% is very high transparency, Sn doped ZnS can be used as a buffer layer for solar cell applications [41]. Reported in that, the effect of the Al doping concentration on ZnS thin films was investigated. According to their results, the optical transmittance changes between 83% and 60% with Al concentration. Thus, we can say Sn-doped ZnS thin films more transparent than Al-doped.

The refractive index n of the films was calculated using the Swane-poel envelope method [42].

$$n = \left[N + (N^2 - s^2)^{1/2} \right]^{1/2} \quad (5)$$

$$N = \left(2s \frac{T_M - T_m}{T_M T_m} \right) + \frac{s^2 + 1}{2} \quad (6)$$

Where $s=1.5$ is the refractive index of the glass substrate, T_M is the transmission maximum and T_m is the corresponding minimum of the spectra.

$$d = \frac{\lambda_1 \lambda_2}{4(\lambda_1 n_2 - \lambda_2 n_1)} \quad (7)$$

Using equation (7), the film thickness was calculated. Where λ_i is the wavelength and n_i is the refractive index at two adjacent extremes. The thicknesses of the films are given in Table 2.

The optical band gap values E_g of the films were calculated using

Tauc model in the high-absorbance region for direct band-gap semiconductor [43].

$$\alpha h\nu = A(h\nu - E_g)^{1/2} \quad (8)$$

Where α is the absorption coefficient, $h\nu$ is photon energy and A is a constant. $(\alpha h\nu)^2$ versus $h\nu$ graph of the films is given in Fig. 5 as inset. It was observed that the optical band gap E_g value decreased by increasing dopant concentration. Table 2 shows the optical parameters of the Sn doped ZnS thin films.

Optical band gap value of the undoped ZnS thin film is in good agreement reported in Ref. [44]. However, our results are different for Sn doped ZnS films reported in Ref. [8]. Despite their results, we reported that the band gap value of the Sn doped films decreased with increased dopant concentration. This may be due to the structural difference. While Sn doped ZnS thin films have a cubic structure in our study, they said that the films preferred hexagonal wurtzite structure. On the other hand, Mn-doped ZnS thin films characteristics were investigated in Ref. [45] and they reported that the optical band gap decreased with increasing Mn doping concentration from 3.66 eV to 3.58 eV. The obtained results close to our results. However, we can say Sn doping concentration is much effective than Mn dopant to reduce the optical band gap value.

3.3. Electrical properties

The dark I-V measurements of undoped and Sn doped ZnS/p-Si

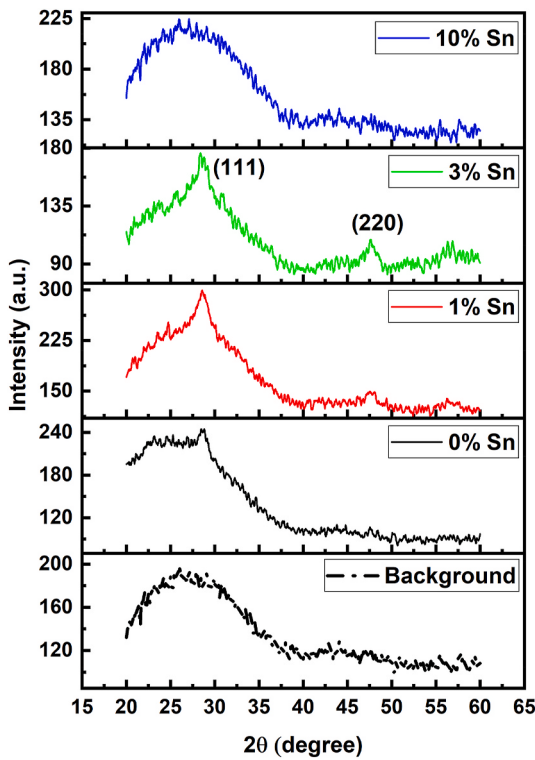


Fig. 2. XRD pattern of Sn doped ZnS thin films.

Table 1
The structural parameters of the undoped and Sn doped ZnS thin films.

	2θ (degree)	D (nm)	d ₁₁₁ (nm)	a (nm)	Δa/a (%)
0% Sn	28.46	10.71	0.313	0.542	0.02
1% Sn	28.58	8.57	0.312	0.540	0.57
3% Sn	28.40	10.70	0.314	0.544	0.17
10% Sn	—	—	—	—	—

junctions were measured as a function of voltage in the range -2 to 2 V at room temperature. Fig. 6 shows the plot of $\ln I$ versus V . It is seen that the undoped and Sn doped ZnS/p-Si junctions exhibit a significant diode behaviour with quite large rectification ratio. The rectification ratio of undoped and Sn doped ZnS/p-Si junctions (defined as the ratio of the forward current to the reverse current) at 2 V is given in Table 3. The rectification ratio increased with %1 ve %3 Sn doping due to decreasing leakage current as shown in Fig. 6.

The electrical properties of undoped and Sn doped ZnS/p-Si diodes as ideality factor and barrier height can be calculated by means of thermionic emission (TE) [46]. According to this theory, the voltage dependence of the forward current is given by the following equation.

$$I = I_0 \left[\exp\left(\frac{qV - IR_s}{nkT}\right) \right] \quad (9)$$

Where I_0 is the saturation current value of the diode and it can be found from the y -intercept value of the $\ln(I)$ versus V graph. The values of n and Φ_b were found from (10) and (11) equations that obtained by rearranging equation (9). The found n and Φ_b values are given in Table 3.

$$n = \frac{q}{kT} \left(\frac{dV}{d(\ln I)} \right) \quad (10)$$

$$\Phi_b = \frac{kT}{q} \ln\left(\frac{AA^*T^2}{I_0}\right) \quad (11)$$

Where A , A^* , T , R_s , k and n are effective diode area (0.025 cm 2),

Richardson constant (32 A/cm 2 K 2 for p-type Si), temperature in Kelvin, series resistance, Boltzmann constant and ideality factor that determines the quality of the diode, respectively.

It can be seen from the table that the barrier heights increased with the Sn contribution. The ideality factor values, on the other hand, decreased with the Sn contribution up to 3% and then increased again at the 10% Sn contribution, but it was still smaller than that of pure ZnS/p-Si diode. Since n values of undoped and Sn doped ZnS/Si diodes are greater than one, they do not exhibit ideal diode behaviour. This may be due to the series resistance [47], interface states [48], non-uniform distribution of the carriers in the interfaces [49] and inhomogeneities of the barrier height [47]. It has been observed that the Sn additive has a positive effect on the diode parameters. The serial resistance is another crucial parameter of diodes that can be calculated using the modified Norde method [50]. Barrier heights can also be calculated from this method. The Norde equation is given below.

$$F(V) = \frac{V}{\gamma} - \frac{kT}{q} \ln\left(\frac{I}{AA^*T^2}\right) \quad (12)$$

$$R_s = \frac{q(\gamma - n)}{kT_{min}} \quad (13)$$

$$\Phi_b = F_{min}(V) + \frac{(\gamma - n)}{n} \left(\frac{V_{min}}{\gamma} - \frac{kT}{q} \right) \quad (14)$$

Where γ is the integer greater than n value of the diode, which obtained from Thermionic Emission method. F_{min} , I_{min} and V_{min} are the minimum points of $F(V)$ versus V plot and corresponding voltage and current values, respectively.

Fig. 7 gives $F(V)$ – V graphs of the diodes. The obtained R_s and Φ_b parameters of diodes are listed in Table 3. Our results are in good agreement with reported results [51,52]. Reported in Ref. [53], Sb doped ZnS nano-Schottky barrier diodes were studied. They obtained the ideality factor of the diodes from 1.31 to 1.39 and barrier height value was deduced from 0.62 to 0.66 eV.

The diodes were illuminated with 100 mW/cm 2 power using AM 1.5 filter. The diodes are light-sensitive because of the current flowing through the structure in the reverse bias region. Fig. 8 shows I–V plots of the diodes at reverse bias region after illumination. As the theory of photovoltaic devices, under illumination reverse current should increase [54]. Thus, we can say that the diodes exhibit photodiode features. When dark and illuminated current values are compared, it can be said that the increase in the current value of the 3% Sn doped diode is greater than the others.

To investigate photodiode characteristic of the devices photosensitivity PS , photoresponsivity R and detectivity D values were calculated using the given equation in below [55,56].

$$PS = \frac{I_{ph}}{I_d} = \frac{I_{ill} - I_d}{I_d} \quad (15)$$

$$R = \frac{I_{ph}}{PxA} \quad (16)$$

$$D = \frac{R}{\sqrt{2qJ_d}} \quad (17)$$

Where I_{ph} , I_{ill} , I_d , P , A and J_d are photocurrent, illuminated and dark current values of the diodes, incident light intensity, active diode area (0.025 cm 2) and dark current intensity, respectively. The photodiode parameters of the structures are given in Table 4 at -1 V bias.

Al-doped n-type ZnS nanowires were studied [57] and the device was illuminated under monochromatic light with varied wavelengths with the intensity 100 μ W/cm 2 . It was reported that the photocurrent was equal to the dark current at the visible region while it increased with decreasing light wavelength. Besides, R values were calculated at 5 V and the best value was found as 4.7×10^6 A/W for 2% doped Al ZnS.

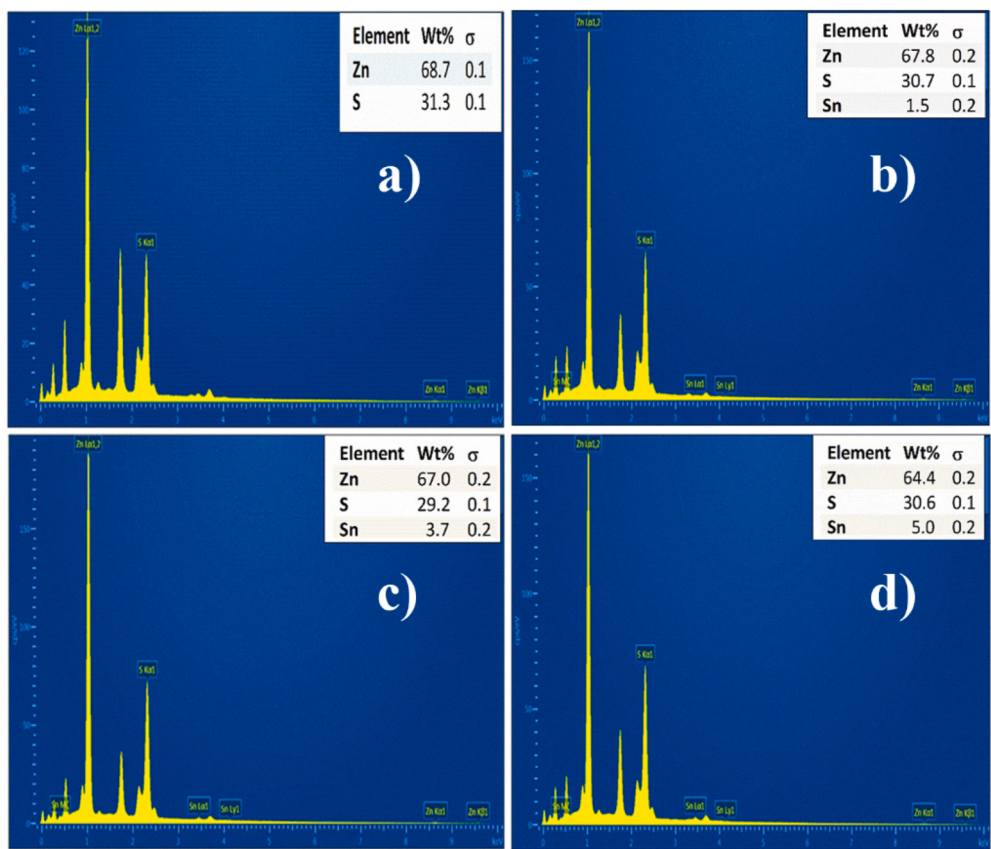


Fig. 3. EDX analysis of Sn doped ZnS (a) 0% Sn, (b) 1% Sn, (c) 3% Sn and (d) 10% Sn.

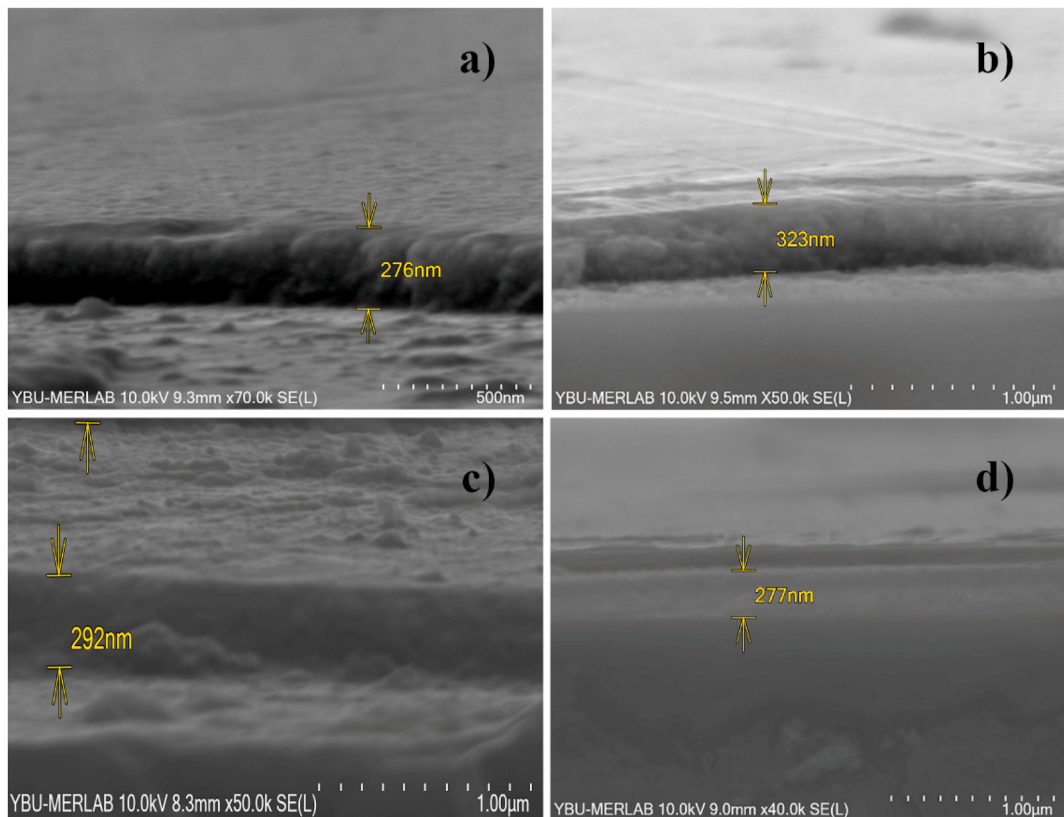
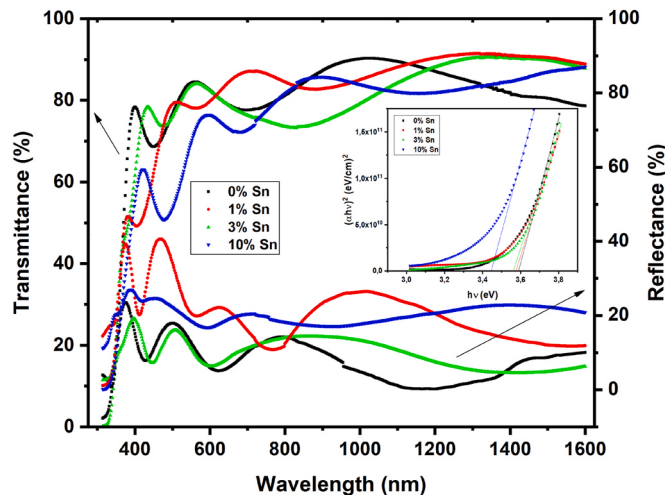
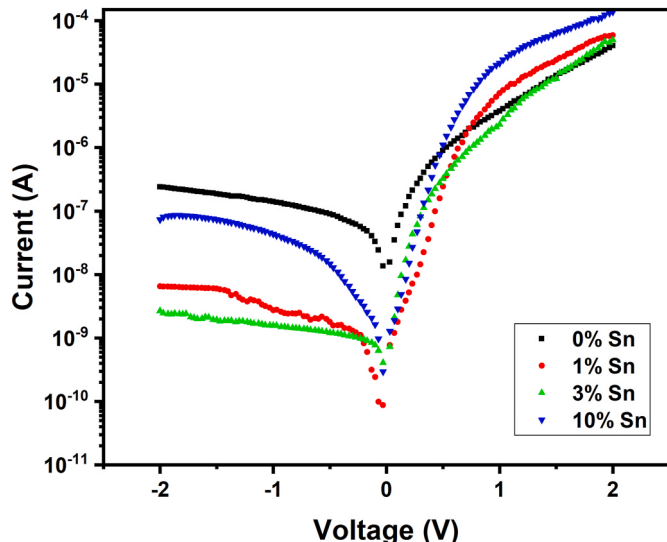


Fig. 4. Cross-sectional SEM images of Sn doped ZnS (a) 0% Sn, (b) 1% Sn, (c) 3% Sn and (d) 10% Sn.

Table 2

Optical parameters of the Sn doped ZnS thin films.

	Thickness (d) (nm) (SEM)	Thickness (d) (nm) (Swanepoel)	Optical band gap (E _g) (eV)
0% Sn	276	284	3.58
1% Sn	323	326	3.55
3% Sn	292	277	3.53
10% Sn	277	290	3.42

**Fig. 5.** Transmittance and reflectance spectrum of the Sn doped ZnS thin films. Inset graph shows $(\alpha h v)^2$ versus $h v$ plot of the films.**Fig. 6.** Semi logarithmic I-V measurements of the undoped and Sn doped ZnS/p-Si junctions.**Table 3**

Diode parameters of the Sn doped ZnS/p-Si structures.

	Rectification Ratio	n	I ₀ (nA)	Φ _b (eV) (TE)	R _s (kΩ)	Φ _b (eV) (Norde)
0% Sn	167.94	3.86	20.95	0.75	41.5	0.74
1% Sn	9062.98	3.71	0.64	0.84	10.5	0.82
3% Sn	18525.91	2.32	0.89	0.83	408	0.82
10% Sn	1876.44	2.36	0.58	0.84	31.5	0.84

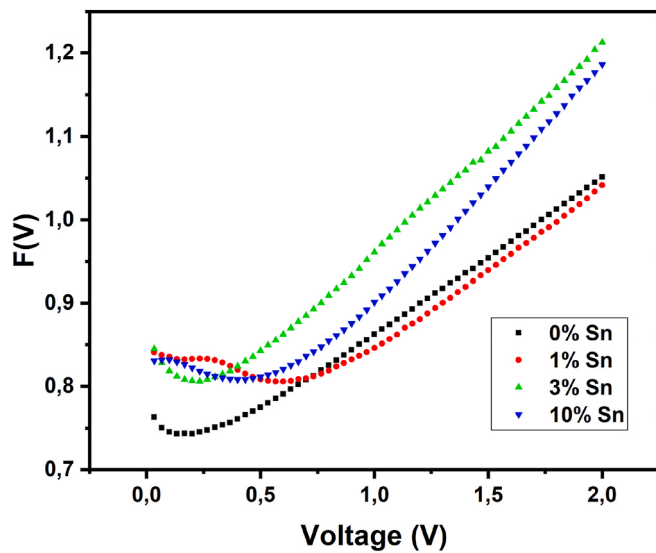
**Fig. 7.** F(V) versus V graph of the Sn doped ZnS/p-Si diodes at room temperature.

Fig. 9 shows responsivity versus reverse bias voltage plot. As the figure, it can be said that responsivity values firstly increased by increasing reverse bias voltage and then responsivity values remained nearly constant for undoped, 1% and 3% Sn doped diodes whereas responsivity values continued to increase for 10% Sn doped diode. On the other hand, it was obtained that 1% and 3% Sn doped diodes responded at a higher voltage value than other diodes. As **Tables 3** and **3%** Sn doped diode has the highest photosensitivity and responsivity values.

4. Conclusion

In summary, undoped and Sn doped ZnS films have been successfully fabricated on glass and p-Si substrates using the sol-gel dip-coating method. XRD results show the films are cubic structure and the main peak intensity has been decreased with increasing Sn concentration. EDX spectrum shows there are no impurities in the ZnS thin film and increasing Sn concentration has decreased Zn concentration of the films. Using cross-sectional SEM images, the film thicknesses have been calculated and these values are very close to found from optical transmittance spectra. The optical band gap values of the thin films have been estimated using optical transmittance spectra. It is seen that Sn concentration reduces the optical band gap value. Besides, the films have very high transparency. Undoped and Sn doped ZnS/Si junctions have been characterized by current-voltage measurement at both dark and illuminated conditions at room temperature. ZnS/p-Si junctions show diode behaviour and photosensitivity. The diode parameters have been investigated using thermionic emission theory and Norde method. The photodiode properties of the devices such as photosensitivity PS, photoresponsivity R and detectivity D have been calculated under 100 mW/cm² illumination. It has been observed that diode parameters and sensitivity change with the contribution of Sn. The 3% Sn doped ZnS/p-Si diode has exhibited both the best correction behaviour and the highest light sensitivity.

CRediT authorship contribution statement

Şirin Uzun Çam: Conceptualization, Investigation, Methodology, Validation, Formal analysis, Visualization, Writing - original draft. **Tülay Serin:** Validation, Formal analysis, Investigation, Resources, Supervision, Writing - review & editing. **A. Necmeddin Yazıcı:** Supervision, Writing - review & editing.

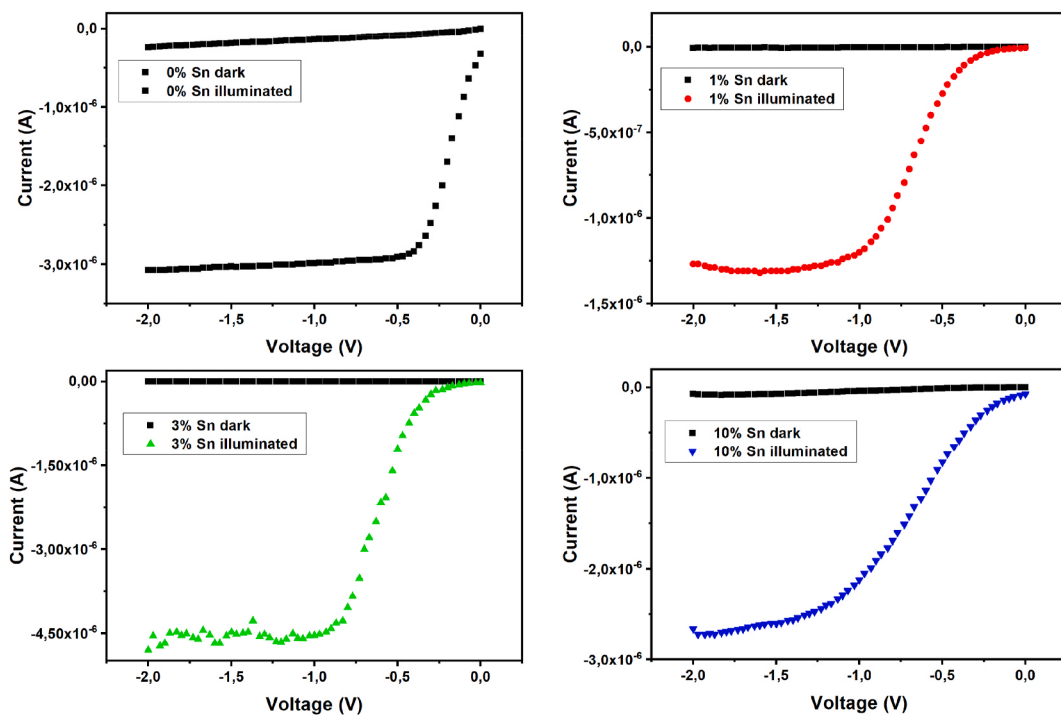


Fig. 8. Illuminated and dark I-V graph of the Sn doped ZnS/p-Si diodes at reverse bias region.

Table 4

Photodiode parameters of the Sn doped ZnS/p-Si structures at -1V bias.

	Photosensitivity (P)	Responsivity (R) (mA/W)	Detectivity (D) (Jones)
0% Sn	20.26	1.14	8.50×10^8
1% Sn	439.04	0.48	25.60×10^8
3% Sn	2900.57	1.81	128.23×10^8
10% Sn	47.66	0.83	11.11×10^8

Declaration of competing interest

The authors declare that they have no known competing financial interests or personal relationships that could have appeared to influence the work reported in this paper.

Acknowledgment

We would like to thank Dr. Ahmet Karatay and Dr. Elif Yıldız for providing illuminated I-V measurements and Abdullah Atılgan for carrying out XRD, EDX and SEM measurements. This work is based on the Sirin Uzun Çam's Ph.D. Thesis.

References

- [1] N. Liu, H. Xue, Y. Ji, J. Wang, ZnSe/ZnS core-shell quantum dots incorporated with Ag nanoparticles as luminescent down-shifting layers to enhance the efficiency of Si solar cells, *J. Alloys Compd.* 747 (2018) 696–702, <https://doi.org/10.1016/j.jallcom.2018.03.060>.
- [2] R.A. Soref, Siliconbased group IV heterostructures for optoelectronic applications, *J. Vac. Sci. Technol.* 14 (1996) 913–918, <https://doi.org/10.1116/1.580414>.
- [3] K.R. Bindu, P.V. Sreenivasan, A.I. Martinez, E.I. Anila, α -Axis oriented ZnS thin film synthesised by dip coating method, *J. Sol. Gel Sci. Technol.* 68 (2013) 351–355, <https://doi.org/10.1007/s10971-013-3177-4>.
- [4] Y. Liu, Y. Sun, W. Liu, J. Yao, Novel high-efficiency crystalline-silicon-based compound heterojunction solar cells: HCT (heterojunction with compound thin-layer), *Phys. Chem. Chem. Phys.* 16 (2014) 15400, <https://doi.org/10.1039/c4cp00668b>.
- [5] S.R. Chalana, R.J. Bose, R.R. Krishnan, V.S. Kavita, R.S. Sreedharan, V.P.M. Pillai, Structural phase modification in Cu incorporated nanostructured zinc sulfide thin films, *J. Phys. Chem. Solid.* 95 (2016) 24–36, <https://doi.org/10.1016/j.jpcs.2016.03.009>.
- [6] X. Yang, B. Chen, J. Chen, Y. Zhang, W. Liu, Y. Sun, ZnS thin film functionalized as back surface field in Si solar cells, *Mater. Sci. Semicond. Process.* 74 (2018) 309–312, <https://doi.org/10.1016/j.mssp.2017.08.011>.
- [7] C. Sabitha, K.D. A Kumar, S. Valaransu, A. Saranya, I. H Joe, Cu:ZnS and Al:ZnS thin films prepared on FTO substrate by nebulized spray pyrolysis technique, *J. Mater. Sci. Mater. Electron.* 29 (2018) 4612–4623, <https://doi.org/10.1007/s10854-017-8412-2>.
- [8] A. Mukherjee, P. Mitra, Characterization of Sn doped ZnS thin films synthesized by CBD, *Mater. Res.* 20 (2) (2017) 430–435, <https://doi.org/10.1590/1980-5373-MR-2016-0628>.

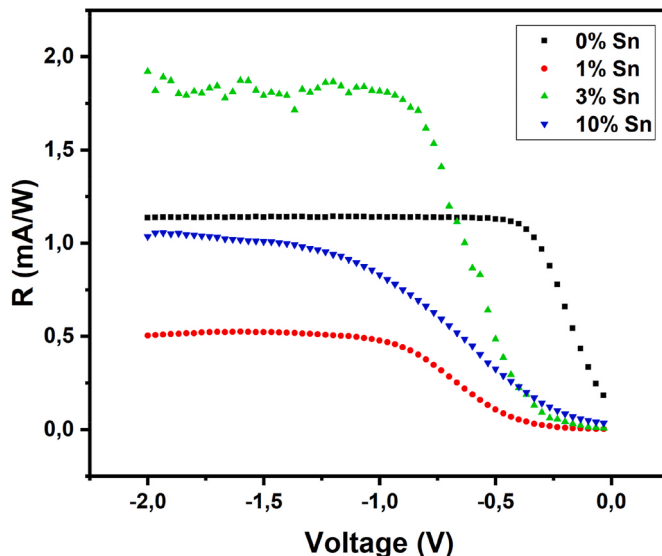


Fig. 9. R versus V graph of the Sn doped ZnS/p-Si diodes at reverse bias.

- [9] A. Göktaş, İ.H. Mutlu, Room temperature ferromagnetism in Mn-doped ZnS nanocrystalline thin films grown by sol-gel dip coating process, *J. Sol. Gel Sci. Technol.* 69 (2014) 120–129, <https://doi.org/10.1007/s10971-013-3194-3>.
- [10] A.N. Yazıcı, M. Öztaş, M. Bedir, The thermoluminescence properties of copper doped ZnS nanophosphor, *Opt. Mater.* 29 (2007) 1091–1096, <https://doi.org/10.1016/j.optmat.2006.04.010>.
- [11] G. Turgut, E.F. Keskenler, S. Aydin, S. Doğan, S. Duman, E. Sönmez, B. Esen, B. Düzgün, A study on characterization of Al/ZnS/p-Si/Al heterojunction diode synthesized by sol-gel technique, *Mater. Lett.* 102–103 (2013) 106–108, <https://doi.org/10.1016/j.matlet.2013.03.125>.
- [12] T.B. Nasr, N. Kamoun, M. Kanzari, R. Bennaceur, Effect of pH on the properties of ZnS thin films grown by chemical bath deposition, *Thin Solid Films* 500 (2006) 4–8, <https://doi.org/10.1016/j.tsf.2005.11.030>.
- [13] A. El Hichou, M. Addou, J.L. Bubendorff, J. Ebothe, B. El Idrissi, M. Troyon, Microstructure and cathodoluminescence study of sprayed Al and Sn doped ZnS thin films, *Semicond. Sci. Technol.* 19 (2004) 230–235, <https://doi.org/10.1088/0268-1242/19/2/018>.
- [14] J. Huang, L. Wang, K. Tang, J. Zhang, R. Xu, Y. Xia, X. Lu, Preparation and properties of n-ZnS film/p-Si heterojunction, *Adv. Mater. Res.* 311–313 (2011) 1277–1280, <http://doi.org/10.4028/www.scientific.net/AMR.311-313.1277>.
- [15] A.K. Katiyar, A.K. Sinha, S. Manna, S.K. Ray, Fabrication of Si/ZnS radial nanowire heterojunction arrays for white light emitting devices on Si substrates, *ACS Appl. Mater. Interfaces* (2014), <https://doi.org/10.1021/am5028605>.
- [16] E.Y.M. Lee, N.H. Tran, R.N. Lamb, Growth of ZnS films by chemical vapor deposition of $\text{Zn}[\text{S}_2\text{C}_2(\text{CH}_3)_2]_2$ precursor, *Appl. Surf. Sci.* 241 (2005) 493–496, <https://doi.org/10.1016/j.apsusc.2004.07.003>.
- [17] Ch Maierhofer, S. Kulkarni, M. Alonso, T. Reich, K. Horn, Valence band offset in ZnS layers on Si (111) grown by molecular beam epitaxy, *J. Vac. Sci. Technol. B* 9 (1991) 2238–2243, <https://doi.org/10.1116/1.585727>.
- [18] H.J. Zhu, Y. Liang, X.Y. Gao, R.F. Guo, Q.M. Ji, Effect of Aluminum doping on the nanocrystalline ZnS:Al³⁺ films fabricated on heavily-doped p-type Si (100) substrates by chemical bath deposition method, *Braz. J. Phys.* 45 (2015) 308–313, <https://doi.org/10.1007/s13538-015-0323-1>.
- [19] E.M. Nasir, Fabrication and characterization of n-ZnS/p-Si and n-ZnS:Al/p-Si heterojunction, *Int. J. Eng. Adv. Technol.* 3 (2013) 425–429.
- [20] I. Tapan, M.A. Ahmetoglu (Afrailov), F. Koçak, A ZnS-Si isotype heterojunction avalanche photodiode structure for scintillation light detection, *Nucl. Instrum. Methods Phys. Res.* 567 (2006) 268–271, <https://doi.org/10.1016/j.nima.2006.05.105>.
- [21] L.W. Ji, Y.J. Hsiao, I.T. Tang, T.H. Meen, C.H. Liu, J.K. Tsai, T.C. Wu, Y.S. Wu, Annealing effect and photovoltaic properties of nano-ZnS/textured p-Si heterojunction, *Nanoscale Research Letters* 8 (2013) 470–475, <https://doi.org/10.1186/1556-276X-8-470>.
- [22] K. Qiu, D. Qiu, L. Cai, S. Li, W. Wu, Z. Liang, H. Shen, Preparation of ZnS thin films and ZnS/p-Si heterojunction solar cells, *Mater. Lett.* (2017), <https://doi.org/10.1016/j.matlet.2017.03.171>.
- [23] Y.J. Hsiao, T.H. Meen, L.W. Ji, J.K. Tsai, Y.S. Wu, C.J. Huang, Preparation of ZnS microdisks using chemical bath deposition and ZnS/p-Si heterojunction solar cells, *J. Phys. Chem. Solid.* 74 (2013) 1403–1407, <https://doi.org/10.1016/j.jpcs.2013.04.023>.
- [24] K.M. Senados, R.M. Vequizo, Effects of thermal annealing on the diode properties and space charge limited conduction of the physical vapor-deposited n-ZnS/p-Si (100) heterojunctions, *Mater. Today: Proceedings* 5 (2018) 15174–15179, <https://doi.org/10.1016/j.mtpr.2018.04.078>.
- [25] N. Nadaud, N. Lequeux, M. Nanot, J. Jove, T. Roisnel, Structural studies of tin-doped indium oxide (ITO) and In₄Sn₃O₁₂, *J. Solid State Chem.* 135 (1998) 140–148, <https://doi.org/10.1006/jssc.1997.7613>.
- [26] S.T. Brevilieri, E.T.G. Cavalheiro, G.O. Chierice, Correlation between ionic Radius and thermal decomposition of Fe(II), Co(II), Ni(II), Cu(II) and Zn(II), *Thermochim. Acta* 356 (2000) 79–84, [https://doi.org/10.1016/S0040-6031\(00\)00465-2](https://doi.org/10.1016/S0040-6031(00)00465-2).
- [27] A.A.A. Ahmed, Z.A. Talib, M.Z. bin Hussein, A. Zakaria, Zn-Al layered double hydroxide prepared at different molar ratios: preparation, characterization, optical and dielectric properties, *J. Solid State Chem.* 191 (2012) 271–278, <https://doi.org/10.1016/j.jssc.2012.03.013>.
- [28] R.D. Shannon, C.T. Prewitt, Revised values of effective ionic radii, *Acta Crystallogr.* 26 (1970) 1046, <https://doi.org/10.1107/S0567740870003576>.
- [29] P.S. Sidhu, R.J. Gilkes, A.M. Posner, The synthesis and some properties of Co, Ni, Zn, Cu, Mn, and Cd substituted magnetites, *J. Inorg. Nucl. Chem.* 40 (1978) 429–435, [https://doi.org/10.1016/0022-1920\(78\)80418-7](https://doi.org/10.1016/0022-1920(78)80418-7).
- [30] R. Bengas, H. Lahmar, K.M. Redha, L. Mentar, A. Azizi, G. Schmerber, A. Dinia, Electrochemical synthesis of n-type ZnS layers on p-Cu₂O/n-ZnO heterojunctions with different deposition temperatures, *RSC Adv.* 9 (2019) 29056, <https://doi.org/10.1039/c9ra04670d>.
- [31] A. Brayek, S. Chaguetmi, M. Ghoul, I. Ben Assaker, R. Chtourou, P. Decorse, P. Beaunier, S. Nowak, F. Mamperi, S. Ammar, The structural and the photoelectrochemical properties of ZnO-ZnS/ITO 1D hetero-junctions prepared by tandem electrodeposition and surface sulfidation: on the material processing limits, *RSC Adv.* 8 (2018) 11785, <https://doi.org/10.1039/c8ra00176f>.
- [32] L.J. Brillson, Y. Lu, ZnO Schottky barriers and Ohmic contacts, *J. Appl. Phys.* 109 (2011) 121301, <https://doi.org/10.1063/1.3581173>.
- [33] H. Farid, M.A. Rafea, E.F. El-Wahiyd, O. El-Shazly, Preparation and characterization of ZnS nanocrystalline thin films by low cost dip technique, *J. Mater. Sci. Mater. Electron.* 25 (2014) 2017–2023, <https://doi.org/10.1007/s10854-014-1790-9>.
- [34] A. Ammar, C. Cros, M. Pouchard, N. Jaussaud, J.-M. Bassat, G. Villeneuve, M. Duttine, M. Menetrier, E. Reny, On the clathrate form of elemental silicon, Si₁₃₆: preparation and characterisation of Na_xSi₁₃₆(x → 0), *Solid State Sci.* 6 (2004) 393–400, <https://doi.org/10.1016/j.solidstatesciences.2004.02.006>.
- [35] M. Ajili, M. Castagne, N.K. Turkı, Study on the doping effect of Sn-doped ZnO thin films, *Superlattice. Microst.* 53 (2013) 213–222, <https://doi.org/10.1016/j.spmi.2012.10.012>.
- [36] R. Mariappan, V. PonnuSwamy, P. Suresh, Effect of doping concentration on the structural and optical properties of pure and tin doped zinc oxide thin films by nebulizer spray pyrolysis (NSP) technique, *Superlattice. Microst.* 52 (2012) 500–513, <https://doi.org/10.1016/j.spmi.2012.05.016>.
- [37] D.E. Ortiz-Ramos, L.A. Gonzalez, R. Ramirez-Bon, p-type transparent Cu doped ZnS thin films by the chemical bath deposition, *Mater. Lett.* 124 (2014) 267–270, <https://doi.org/10.1016/j.matlet.2014.03.082>.
- [38] F. Kurnia, Y. Hau Ng, Y. Tang, R. Amal, N. Valanoor, J.N. Hart, ZnS thin films for visible-light active photoelectrodes: effect of film morphology and crystal structure, *Cryst. Growth Des.* 16 (5) (2016) 2461–2465, <https://doi.org/10.1021/acs.cgd.5b01590>.
- [39] T. Serin, S. Gürkar, N. Serin, N. Yıldırım, F.Ö. Kuş, Current flow mechanism in Cu₂O/p-Si heterojunction prepared by chemical method, *J. Phys. Appl. Phys.* 42 (5pp) (2009) 225108, <https://doi.org/10.1088/0022-3727/42/22/225108>.
- [40] T.K. Pathak, V. Kumar, L.P. Purohit, H.C. Swart, R.E. Kroon, Substrate dependent structural, optical and electrical properties of ZnS thin films grown by RF sputtering, *Physica E* 84 (2016) 530–536, <https://doi.org/10.1016/j.physE.2016.06.020>.
- [41] H. Benamra, H. Saidi, A. Attaf, M.S. Aida, A. Derbali, N. Attaf, Physical properties of Al-doped ZnS thin films prepared by ultrasonic spray technique, *Surfaces and Interfaces* 21 (2020) 100645, <https://doi.org/10.1016/j.surfin.2020.100645>.
- [42] R. Swanepoel, Determination of the thickness and optical constants of amorphous silicon, *J. Phys. E Sci. Instrum.* 16 (1983) 1214–1223.
- [43] J. Tauc, Optical Properties of Solids, North-Holland Publ., vol. 279, Amsterdam.
- [44] A. Göktas, F. Aslan, E. Yaşar, I.H. Mutlu, Preparation and characterisation of thickness dependent nano-structured ZnS thin films by sol-gel technique, *J. Mater. Sci. Mater. Electron.* 23 (2012) 1361–1366, <https://doi.org/10.1007/s10854-011-0599-z>.
- [45] D. Talantikite-Touati, H. Merzouk, H. Haddad, A. Tounsi, Effect of dopant concentration on structural and optical properties Mn doped ZnS films prepared by CBD method, *Optik* 136 (2017) 362–367, <https://doi.org/10.1016/j.ijleo.2017.02.032>.
- [46] S.M. Sze, Physics of Semiconductor Devices, second ed., John Wiley & Sons Publ, 1981, pp. 850–860.
- [47] M. Gökçen, T. Tunç, Ş. Altindal, İ. Uslu, The effect of PVA (Bi₂O₃-doped) interfacial layer and series resistance on electrical characteristics of Au/n-Si (110) Schottky barrier diodes (SBDs), *Curr. Appl. Phys.* 12 (2012) 525–530, <https://doi.org/10.1016/j.cap.2011.08.012>.
- [48] Ş. Aydoğan, M.L. Grilli, M. Yılmaz, Z. Çaldırın, H. Kaçış, A facile growth of sprayed based ZnO films and device performance investigation for Schottky diodes: determination of interface state density distribution, *J. Alloys Compd.* 708 (2017) 55–66, <https://doi.org/10.1016/j.jallcom.2017.02.198>.
- [49] Y.X. Luo, C.H. Shih, Coupling of carriers injection and charges distribution in Schottky barrier charge-trapping memories using source-side electrons programming, *Semicond. Sci. Technol.* 29 (2014) 115006, <https://doi.org/10.1088/0268-1242/29/11/115006>.
- [50] H. Norde, A modified forward I-V plot for Schottky diodes with high series resistance, *J. Appl. Phys.* 50 (1979) 5052–5053.
- [51] H.K. Kaplan, S. Sarıç, S.K. Akay, M. Ahmetoglu, The characteristics of ZnS/Si heterojunction diode fabricated by thermionic vacuum arc, *J. Alloys Compd.* 724 (2017) 543–548, <https://doi.org/10.1016/j.jallcom.2017.07.053>.
- [52] A. Ateş, B. Güzeldir, M. Sağlam, ZnS thin film and Zn/ZnS/n-Si/Au-Sb sandwich structure grown with SILAR method and defining the characteristic parameters, *Mater. Sci. Semicond. Process.* 14 (2011) 28–36, <https://doi.org/10.1016/j.mssp.2010.12.014>.
- [53] Q. Peng, J. Jie, C. Xie, L. Wang, X. Zhang, D. Wu, Y. Yu, C. Wu, Z. Wang, P. Jiang, Nano-Schottky barrier diodes based on Sb-doped ZnS nanoribbons with controlled p-type conductivity, *Appl. Phys. Lett.* 98 (2011) 123117, <https://doi.org/10.1063/1.3569590>.
- [54] F. Yakuphanoglu, Y. Caglar, M. Caglar, S. Ilican, ZnO/p-Si heterojunction photodiode by sol-gel deposition of nanostructure n-ZnO film on p-Si substrate, *Mater. Sci. Semicond. Process.* 13 (2010) 137–140, <https://doi.org/10.1016/j.jallcom.2010.05.005>.
- [55] O. Dayan, A.G. Imer, A.G. Al-Shehmi, N. Özdemir, A. Dere, Z. Şerbetçi, A.A. Al-Ghamdi, F. Yakuphanoglu, Photoresponsivity and photodetectivity properties of copper complex-based photodiode, *J. Mol. Struct.* 1200 (2020) 127062, <https://doi.org/10.1016/j.molstruc.2019.127062>.
- [56] K. Ozel, A. Atilgan, N.E. Koksal, A. Yildiz, A route enhanced UV photo-response characteristics of SnO_x/p-Si based heterostructures by hydrothermally grown nanorods, *J. Alloys Compd.* 849 (2020) 156628, <https://doi.org/10.1016/j.jallcom.2020.156628>.
- [57] P. Jiang, J. Jie, Y. Yu, Z. Wang, C. X, X. Zhang, C. Wu, L. Wang, Z. Zhu, L. Luo, Aluminium-doped n-type ZnS nanowires as high-performace UV and humidity sensors, *J. Mater. Chem.* 22 (2012) 6856, <https://doi.org/10.1039/c2jm15365c>.